Research paper

Rational steel mesh layout influence on plate utilization of large span corrugated steel structure

Nerijus Bareikis[1]

Abstract: Corrugated steel structures buried in the surrounding soil are currently used worldwide in road and railway engineering as culverts, pedestrian and animal crossings, tunnels and bridges. The need of large span corrugated steel structures is rapidly growing however their behavior analysis is still understudied. There is also a lack of discussion about the impact of additional strengthening elements for the behavior of corrugated steel structures. This study analyses the influence of rational steel mesh layout on the behavior of a large span deepest corrugation steel structure. The numerical two-dimensional model of two-radius 17.5 m span profile with corrugation of 237 mm depth and 500 mm pitch was developed to replicate the ongoing project in Lithuania. Originally the stiffness of the structure from both sides was increased by six layers of steel meshes as lateral support. Nevertheless, the current study was looking for rational steel mesh layout. Also, the influence of different layouts of steel mesh on corrugated steel plate utilization to buckling failure in the peaking, dead load and in the most unfavorable live load location phase was analyzed. The finite element model results indicated that steel meshes could be used to control structure deformations and internal reactions. Vertical displacement of the crown of the structure could be reduced by 45% in the peaking phase when using proper steel meshes layout. Furthermore, steel meshes could be a decisive factor for the bearing capacity of corrugated steel structure in a positive sense.

Keywords: corrugated steel structure, finite element, large span, nonlinear analysis, soil steel composite bridge, strengthening elements

---

[1]PhD Student, Vilnius Gediminas Technical University, Faculty of Civil Engineering, Saulėtekio al. 11, LT-10223 Vilnius, Lithuania, e-mail: nerijus.bareikis@vilniustech.lt, ORCID: 0009-0006-6744-0782

1. Introduction

Almost 200 years passed when corrugated steel plates were used in construction for the very first time. Henry Robinson Palmer (1795–1844) was a British civil engineer who was credited as the inventor of corrugated metal roofing [1]. Although it was originally made from the wrought iron it proved to be light, strong, corrosion-resistant, and easily transported. Today corrugated steel plates are made by highly automated production process of a roll forming and they are used in various applications of construction of civil and road engineering. Corrugated steel pipes and structures in road and railway engineering are currently used worldwide as culverts, pedestrian and animal crossings, tunnels and bridges under all types of variable live loads (LL). Corrugated steel structures (CSS) already proved their advantages because of an interaction with surrounding soil, but development of the technology is far from stopping. The demand of large span CSS is growing very fast while their behavior analysis is still not studied in detail and not fully covered in Canadian Highway Bridge Design Code (CHBDC) [2], American Association of State Highway and Transportation Officials (AASHTO) [3] or Swedish Design Method (SDM) [4–6] design manuals. Steel plate properties, corrugation and soil parameters in most of the cases are decisive for the CSS bearing capacity. However, in some of the cases large span CSS strength utilization requires additional strengthening elements [7] and the lack of in-depth investigation of such combined system makes the design process even more complicated.

For the past decade CSS behavior was extensively studied by monitoring its performance under dead and live load influence [8–17]. A few full-scale destructive tests were performed to investigate the causes of collapse with the aim of improving calculation methods [8, 18–22]. A significant amount research for various purposes simulated CSS performance in a two-dimensional or three-dimensional space numerically [19, 23–29]. Nevertheless, only a small proportion of the research was conducted comprehensively considering the impact of different strengthening elements for CSS behavior [7, 28, 30–34]. Moreover, none of the investigations evaluated the influence of the reinforcement materials as a possibly better performance alternative to the increase of thickness of the steel plate to attain CSS global stability.

The effectiveness of lateral reinforced steel mesh and circumferential steel stiffeners were analyzed for the world's largest span CSS of 32.40 m and vertical height of 9.57 m [7]. Field measurements were employed to validate three-dimensional finite element model (FEM) which was later used to evaluate the influence of strengthening techniques for buried steel structure. FEM results revealed that steel meshes reduced the induced straining actions in CSS up to 50%. In addition, it was concluded that the circumferential steel stiffeners could be used to control crown vertical deformations less than 0.5% of the structure rise during and after construction. However, steel mesh properties and configuration same as the layout was not investigated in detail with respect to the steel mesh resistance to tension and to steel mesh influence on CSS bearing capacity. Moreover, the effect of the variable live load was not in the scope of the study.

Continued research by the same authors was performed investigating bevel-ended world's largest span CSS [30]. The study is related to the fact that buried steel structures encounter beveling slopes as per design requirements although it is an extremely complicated configuration of CSS for the empirical evaluation. However, the stability of buried steel structure shell is critical because of lateral soil pressure where the steel plates do not consist of full

ring. The results of the research indicated that the significant longitudinal bending moment induced in the steel plates which were not supported by the full ring. Longitudinal bending moment increased significantly by increasing the slope of the beveled ends. Finally, it was concluded that steel meshes around CSS reduce circumferential axial stresses by up to 30%. Nevertheless, the concrete collar compared to other strengthening techniques controlled the design and demonstrated the greatest influence reducing the longitudinal bending moment. Notwithstanding, the influence of the different steel mesh layouts was not investigated in the study. Rational steel mesh layout and concrete collar parameters in respect to the steel plate utilization were not considered in the study too.

In the current study numerical model of a large span deepest CSS interaction with a surrounding soil mass and different layout of the steel meshes as additional strengthening material were analyzed. The study seeks to investigate the corrugated steel plate interaction with different layout of the steel meshes not focusing on the influence of the soil different properties (study does not focus on the geotechnical limit state). The main objective of this investigation is to present the influence of different layouts of the steel mesh on the CSS plate utilization. Moreover, this study presents the setup of rational steel mesh characteristics and their rational layout. To achieve these objectives a two-dimensional nonlinear finite element model was generated with the help of Plaxis 2D software [35]. Two-radius CSS profile with a span of 17.5 m was chosen for a numerical simulation considering it as one of the most commonly applicable profile in the east European countries over the two lanes road. The study examines structural response in the three phases: peaking, full dead load (DL) of 1.4 m soil cover above the crown of the structure and most unfavorable position of LM1 live load model according to the EN 1991-2 standard requirements.

2. Description of the structure

The two-radius CSS profile with a span of 17.5 m and a rise of 5.2 m in the axis were designed in Lithuania above Kaunas city bypass in 2022. Such a profile was chosen as the most suitable profile to keep the clearance box of 10 m width and 5.2 m height as per national regulation requirements for the two lanes highway with a possibility to extend the road adding one additional line in perspective. A road above CSS of 9 m width between guardrails including two opposite direction lanes of 4 m width was designed in the project. However, the design task requested longer CSS of 22 m in axis for road network development in perspective. CSS ends were cut vertically with a posibility to install reinforced concrete retaining walls in the future. As per design, the deepest corrugation profile (500 mm pitch ×237 mm depth) of 8.0 mm steel plate was necessary for the 1.4 m soil cover and LM1 live load model. To increase the stiffness of CSS the six layers of steel meshes were introduced as a lateral support. The steel mesh reinforcement of 10 mm steel bars spaced every 200 mm were situated in the longitudinal direction and the secondary reinforcement of 8 mm steel bars spaced every 800 mm were connected to the main reinforcement in the transverse direction. The vertical distance between steel mesh layers was not equal and ranged between 800 mm and 400 mm as presented. The first layer of steel mesh was placed at 2.0 m distance measuring from the top of the concrete

foundation. Anchoring length of all steel mesh layers was 5.2 m measuring from CSS support point. Steel meshes were connected to CSS at the places of bolted plate connections. The structure was supported on 10 m long 800 mm diameter reinforced concrete piles spaced every 1.0 m. On the top of the piles 1.5 m width and 2.25 m height solid pile heads were necessary by the design. The concrete class of C30/37 was designed according to the EN 206 standard requirements to support vertical and horizontal reactions redistributed by CSS. According to the design steel structure will be backfilled with the granular soil material of sand-gravel mix with less than 5% fines. Unit weight of backfill soil should be 21.50 kN/m^3 and effective friction angle of 33 degrees. The sieve curve of backfill soil should present the uniformity coefficient $C_u > 6$ and the curvature coefficient C_c in a range between 1 and 3. According to the triaxial test results deformation modulus E_{50} for backfill material should be close to 35 MPa when $\sigma_3 = 100$ MPa. The backfill aggregate must be compacted every 300 mm thick layers up to 98% of standard Proctor test. Figure 1 presents a transverse view of the CSS and steel meshes layout designed in the project.
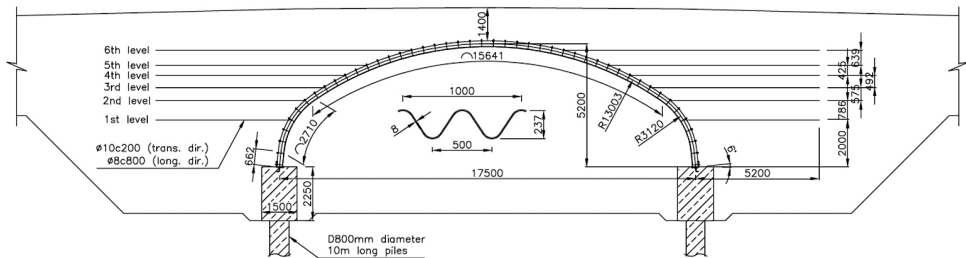
Fig. 1. Transverse section of CSS of Kaunas city bypass (all dimensions in mm)

3. Numerical model

A two-dimensional nonlinear finite element plane strain model was generated using Plaxis 2D software [35]. Taking into account the main objectives of the article and the location of the 9 m width road above the CSS (when LL is far enough from the ends of the CSS) it was not necessary to build a 3D model to achieve the results and draw the conclusions. CSS profile cross section in the position of road longitudinal axis was analyzed in the article and the impact retaining wall on the edges of the structure was neglected. Nevertheless, the results of 2D problem idealization of a plane strain model concept could be compared with 3D model results, but it is not a part of this article. Figure 2 presents the transfer section of the structure developed in a software.

The boundary conditions of the model were limited accordingly: horizontally five times of the span of the steel structure and vertically below foundations one and a half times of the pile length. Steel structure, concrete piles and pile heads were modeled as plate elements. Steel meshes were modelled with a use of geogrid elements without any additional constraints. The soil elements were simulated as 15-node triangles. Separate soil regions were introduced for
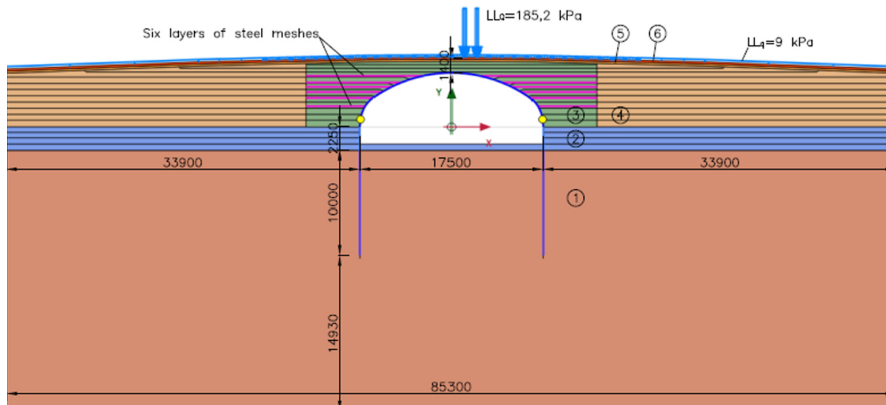
Fig. 2. Numerical model details and dimensions in mm (soil layers numbering conform to Table 1)

native soil, foundation backfill, engineering backfill, embankment and road superstructure. Engineering backfill envelope was assumed according to the AASHTO [3] regulations. Interface elements were introduced between soil and all plate and geogrid (steel mesh) elements. The interface resistance factor was assumed as 0.8 for non-cohesive soils [36]. Numerical model finite element mesh is shown in Fig. 3.
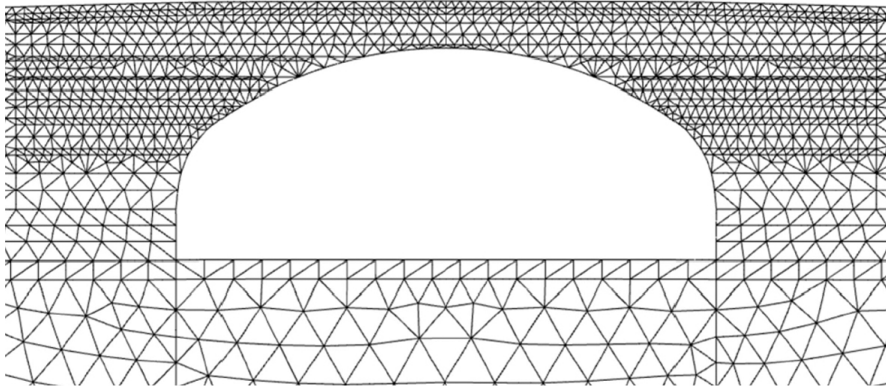
Fig. 3. Numerical model finite element mesh

Equivalent stiffness and unit weight values were determined in the 2D software for plate elements to meet corrugated steel cross section and concrete foundation parameters. Equivalent stiffness of geogrids representing steel meshes were calculated according to the layout of longitudinal steel bars. It was assumed that transfer steel bars were used only to build the meshes and their influence on the results is negligible. Table 1 shows plate element and geogrid material properties used in this paper.

Mohr–Coulomb soil model was assumed for simulating the performance of the native soils and backfill materials. Linear elastic soil model was set for asphalt layer while steel

Table 1. Summary for soil and structure material properties

No	Identification	Material model type	Unit weight	Elastic modulus	Poisson's ratio	Cohesion	Friction angle	Yield stress
			kN/m^3	MPa	–	kPa	Degrees	MPa
1	Subsoil	Mohr–Coulomb	21.5	120	0.20	1	30	–
2	Foundation backfill	Mohr–Coulomb	21.2	80	0.23	1	29	–
3	Engineering backfill	Mohr–Coulomb	21.5	35	0.20	0	33	–
4	Embankment	Mohr–Coulomb	21.2	30	0.23	1	29	–
5	Road subbase	Mohr–Coulomb	23.0	400	0.23	1	43	–
6	Asphalt	Linear elastic	23.0	400	0.40	–	–	–
7	Foundation concrete	Elastic	21.6	30000	0.20	–	–	–
8	Corrugated steel shell	Elastic	78.5	210000	0.30	–	–	420
9	Geogrids as steel meshes	Elastic	78.5	210000	0.30	–	–	500

plate, concrete foundation elements and geogrids – elastic type of material. Table 1 shows soil properties assumed in the current study which were based on the properties specified in the design project also considering geotechnical survey of native soil, national regulation requirements and engineering experience in the design of CSS. Current study seeks only to analyze corrugated steel plate behavior because of the impact of steel meshes regardless of the influence of different soil properties. However, geotechnical consideration is certainly an important aspect in the design process of CSS [37].

Twenty-two phases representing different backfill heights around the CSS were analyzed to repeat as much as possible realistic construction stages on the site. The thickness of backfill layers was increased up to 60 cm as the lower layer thickness did not have significant influence on the results. During calculations one soil layer difference at the sides of CSS was considered to evaluate an influence of unsymmetrical loading. Soil compaction load was not simulated evaluating the usage of only light compaction equipment.

According to EN 1991-2 the tandem system of LM1 live load model (dynamic amplification included) was placed on different positions over the CSS to find most unfavorable location. Thirty additional phases were created simulating LL movement above the structure in perpendicular direction to CSS axis. In each phase LL was moved by 1.2 m starting from the position of 9.5 m

measuring from the foundation axis. Influence of LL position further from the foundation was neglectable small. Figure 4 represents LL position straight above the CSS crown. Most unfavorable position of LL is shown in Fig. 2.
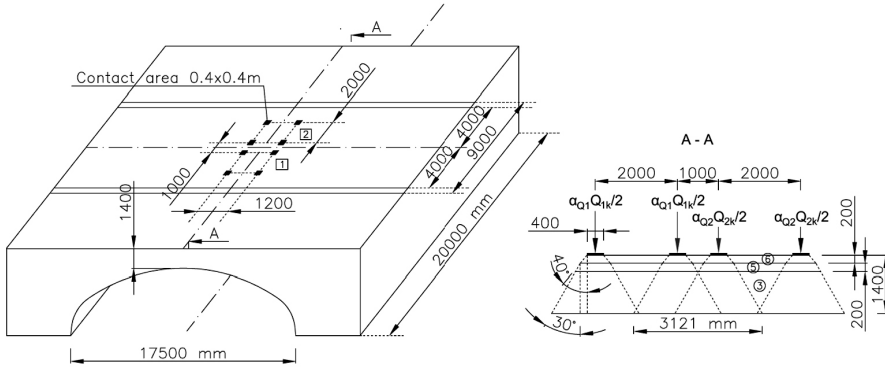
Fig. 4. Live load model LM1 layout in a position above the CSS crown
(soil layers numbering conform to Table 1)

Because of 2D problem idealization of a plane strain model only two wheels were introduced in the model. LL distribution in transverse plane direction of the road axis was calculated according to AASHTO [3] recommendations since LL footprint in that direction is confined to a unit slice. The Reduced Surface Load (RSL) procedure is used for correcting 2D plane strain model where the surface pressure is reduced by reduction factor [38]. According to Ad-hoc method specified in AASHTO [3] regulations such reduction factor for the interaction of two wheels on a single axis in transverse plane direction of the road axis could be calculated by the equation Eq. (3.1) which is already adopted to LM1 LL in this article.

$$(3.1) \quad LL_Q = r(H)P_0 = \frac{2W_0}{S} + W_0 + 2\tan\theta \cdot HP_0 = \frac{\alpha_{Q1} \cdot Q_{1k}/2 + \alpha_{Q2} \cdot Q_{2k}/2}{(S + W_0 + 2\tan\theta \cdot H) \cdot W_0} =$$
$$= \frac{0.8 \cdot 150 + 1.0 \cdot 100}{3.121 \cdot 0.4} = 176.2 \text{ kPa}$$

where: LL_Q – live load model LM1 pressure of two wheels interaction on a single axis (according to Fig. 4 section A–A minimal distance of 1.0 m is between first line wheels and second line wheels, so such interaction will generate highest pressure and the rest LL axles can be neglected), $r(H)$ – surface pressure reduction factor according to AASHTO [3] Ad-hoc method, P_0 – actual service pressure on the footprint, W_0 – footprint width (equal to 0.4 m according to Fig. 4 section A–A), S – minimal spacing between wheels (equal to 1.0 m according to Fig. 4 section A–A), θ – load distribution angle (equal to 40° for asphalt layer and to 30° for all other soil layers according to Fig. 4 section A–A), H – height of cover (equal to 1.4 m), α_{Q1} and α_{Q2} – live load adjustment factor for first and second lane (equal to 0.8 for first lane and 1.0 for second lane according to EN 1991-2), Q_{1k} and Q_{2k} – axle load for first and second lane (equal to 300 kN and 200 kN according to EN 1991-2).

To consider wheels loading in the transverse plane direction of the road axis 185.2 kPa pressure under two 0.4 m width wheels was defined in Plaxis FE model as presented in Fig. 2. Wheels pressure also includes uniformly distributed load of 9 kPa which is also placed on the whole asphalt surface according to EN 1991-2. In the longitudinal direction of the road axis the increasing footprint length as soil depth increases is correctly simulated by the 2D model.

Structural response of the three main stages was examined in the study: peaking (16), full dead load (22), and most unfavorable position of live load (39). Peaking stage is a stage where maximum upward displacement of the crown point of the structure occurs. Usually, peaking stage occurs when the backfill reaches the crown point of the structure. Full dead load stage is usually the last stage when all soil layers are activated. The tandem system of LL at the most unfavorable position (as shown in Fig. 2) is a stage when interaction of axial force and bending moment has the highest influence on CSS plate utilization.

4. Numerical modeling results and discussion

In order to investigate what is the influence of steel meshes to CSS and does rational steel mesh layout will allow to reduce CSS plate thickness it was decided: firstly, to find rational steel mesh parameters and their rational layout concerning mesh resistance to tension and secondly, to analyze results of the steel plate utilization to buckling failure according to AASHTO [3] and Eurocode (EC) [39] in combination with SDM [6] regulations. Respectively the following principal equations Eq. (4.1) and Eq. (4.2) were used for plate utilization calculations.

Buckling failure according to AASHTO [3] regulations:

$$(4.1) \qquad R_b = 1,2\varphi_b C_n (E_p I_p)^{1/2} (\varphi_s M_s K_b)^{2/3} R_h$$

where: R_b – nominal axial force in culvert wall to cause general buckling, φ_b – resistance factor for general buckling, C_n – scalar calibration factor to account for some nonlinear effects (equal to 0.55), E_p – modulus of elasticity of pipe wall material, I_p – moment of inertia of stiffened culvert wall per unit length, φ_s – resistance factor for soil, M_s – constrained modulus of embedment, $K_b = (1 - 2\nu)/(1 - \nu^2)$, ν – Poisson's ratio of soil, R_h – correction factor for backfill geometry $R_h = 11.4/(11 + S/H)$, S – culvert span, H – depth of fill over top of culvert.

Development of plastic hinge in the crown of the structure according to SDM [6]:

$$(4.2) \qquad \frac{N_{Ed}}{\dfrac{\chi_y N_{Rk}}{\gamma_{M1,\text{steel}}}} + k_{yy} \frac{M_{y,Ed}}{\dfrac{M_{y,Rk}}{\gamma_{M1,\text{steel}}}} \leq 1.0$$

where: N_{Ed} and $M_{y,Ed}$ – design value for axial force and bending moment, χ_y – reduction factor for flexural buckling $\chi_y = N_{cr}/N_u$, N_{cr} – buckling load for a buried pipe, N_u – normal force capacity of a fully plasticized cross-section, k_{yy} – interaction factor, N_{Rk} and $M_{y,Rk}$ – resistance for axial force and bending moment $N_{Rk} = f_y A$ and $M_{y,Rk} = f_y W$, f_y – steel material yield stress, A – cross-sectional area, W – section modulus, $\gamma_{M1,\text{steel}}$ – material partial coefficient for steel.

It is important to mention that both standardized approaches mentioned above are not dedicated for the CSS reinforced with steel meshes buckling to failure calculations. A more detailed analysis considering "bracing effect" is necessary to present the influence of steel meshes for the CSS structural behavior.

Three criteria were considered looking for rational steel mesh parameters and layout: diameter and spacing of main longitudinal reinforcement, quantity of steel mesh layers and steel meshes length (anchorage length). All iterations were done for 8 mm steel plate thickness of CSS. Results of steel plate utilization were compared with a model without any steel meshes same for 8 mm and 7 mm steel plate. In addition, one more iteration was generated for 7 mm steel plate with rational steel mesh layout to compare the results. In total 16 numerical models (iterations) with different layouts of steel meshes as presented in Table 2 were analyzed in this paper.

Table 2. Number of iterations of different layouts of steel meshes analyzed in the study and their utilization to maximum tension force according to FEM results

Iteration	Steel mesh layout	Steel mesh utilization to maximum tension force
It1	t-8, no steel meshes	–
It2	t-8, d10c200, 6ly, L-5.2	0.692
It3	t-8, d10c250, 6ly, L-5.2	0.772
It4	t-8, d6c250, 6ly, L-5.2	1.344
It5	t-8, d14c200, 6ly, L-5.2	0.485
It6	t-8, d8c200, 6ly, L-5.2	0.855
It7	t-8, d8c200, 1ly2l, L-5.2	0.683
It8	t-8, d8c200, 1ly5l, L-5.2	1.151
It9	t-8, d8c200, 2ly2l5l, L-5.2	1.155
It10	t-8, d8c200, 3ly2l5l6l, L-5.2	1.034
It11	t-8, d8c200, 3ly2l4l5l, L-5.2	0.969
It12	t-8, d8c200, 3ly2l4l5l, L-3.9	0.970
It13	t-8, d8c200, 3ly2l4l5l, L-1.9_2l, L-2.7_4l5l	0.971
It14	t-8, d8c200, 3ly2l4l5l, L-0	0.927
It15	t-7, d8c200, 3ly2l4l5l, L-1.9_2l, L-2.7_4l5l	0.994
It16	t-7, no steel meshes	–

where: t-8 – CSS steel plate thickness of 8 mm; d8c200 – steel mesh longitudinal steel bar diameter of 8 mm and spacing between bars of 200 mm; 3ly2l4l5l – in total three layers (3ly) activated in the model at 2nd, 4th and 5th level (see Fig. 5); L-1,9_2l – second level steel mesh anchorage length of 1.9 m (see Fig. 5).

Fig. 5. Rational steel mesh layout as assumed in iteration No 13 presented in Table 2 (all dimensions in mm)

4.1. Rational steel mesh layout

In the first iteration of FE model with steel meshes (iteration No 2) diameter and spacing of longitudinal steel bars was set to 10 mm c/c 200 mm accordingly. Six steel mesh layers and steel mesh length of 5.2 m measuring from CSS support point was set as a default in the first iteration as per initial project requirements (see Fig. 1). The ultimate tension resistance of such steel mesh layout was utilized to 69.2%. The highest percentage of utilization of 85.5% was received only with 8 mm diameter spaced every 200 mm longitudinal steel bars (iteration No 6). It was the most accurate approximation considering maximum tension force of 90 kN/m from FE model results. The diameter and spacing of main longitudinal reinforcement were the first criterion of steel mesh rationalization. Steel mesh utilization results also for intermediate iterations are presented in Table 2.

The second criterion of steel mesh rationalization was the quantity of steel mesh layers. It is important to mention that every next iteration was done with the same layout of longitudinal steel bars of 8 mm c/c 200 mm. Originally the six steel mesh layers on every side of the structure were designed in the project. However, according to the results 2nd, 4th, and 5th layers were most significant and took over the highest tension force values with utilization of 96.9% (iteration No 11). The second layer of steel mesh experienced the highest tension force in the peaking phase of the structure while the 4th and 5th layers – during the combination of the full DL and LL phase. All other layers (1st, 3rd and 6th) took over only the part of tension force from neighborhood layers and as later results will show their influence on CSS behavior was minor.

The last steel mesh rationalization criterion was the steel mesh anchorage length. In the project steel mesh length from support point was equal to 5.2 m and it was in the range of engineering backfill (see Fig. 1). During a few iterations with the different steel meshes length it was noticed that anchorage length according to FEM results had very small influence on the utilization of steel mesh by itself. However, as the following results will show, even a very small steel mesh length (0 m from the support point) had influence on the behavior of CSS. Such FEM results are questionable considering embankment over the structure settlements because of deformations of the structure. Soil area straight above the structure could be assigned to the active zone as per instructions of mechanically stabilized earth (MSE) wall calculations listed in the British standard [40]. Without reinforcement the active zone is unstable and tends to move outwards and downwards with respect to the resistant zone. Considering what was said, FEM with small anchorage length results could be justified or rejected by the field test. Nevertheless,

it was decided to calculate steel mesh anchorage length according to the British standard [40] resistance of reinforcing element adherence equation Eq. (4.3) and to set such steel mesh length as rational for the further analysis. According to the calculations anchorage length of the 2nd layer of steel mesh should be 1.9 m and 2.7 m for 4th and 5th steel mesh layers. Utilization of such steel mesh layout as in iteration No 13 presented in Table 2 is 97.1%. It is assumed that such steel mesh layout is rational with respect to resistance to maximum tension force.

$$(4.3) \qquad P_j \geq \frac{T_j}{\dfrac{\mu L_{ej}(f_{fs}\gamma_1 h_j + f_f w_s)}{f_p f_n} + \dfrac{a'_{bc}c'L_{ej}}{f_{ms}f_p f_n}}$$

where: P_j – total horizontal width of the top and bottom faces of the reinforcing element at the jth layer, T_j – maximum tensile force rom FEM results, μ – coefficient of friction between the fill and reinforcing elements, L_{ej} – length of reinforcement in the resistant zone outside failure wedge, at the jth layer of reinforcements, f_{fs} – partial load factor applied to soil self-weight, h_j – depth of the elements below the top of the structure, f_f – partial load factor applied to surcharge dead loads, w_s – surcharge due to dead loads only, f_p – partial factor for reinforcement pull-out resistance, f_n – partial factor applied to economic ramifications of failure, a'_{bc} – adhesion coefficient between the soil and the reinforcement, c' – cohesion of the soil measured under effective stress conditions, f_{ms} – partial material factor.

4.2. Steel mesh influence on CSS

Below results present direct influence of rational steel meshes layout to CSS in peaking, DL and in the most unfavorable location of LL phase. CSS crown total displacements u_y are mostly affected by steel meshes in the peaking phase (see Fig. 6).
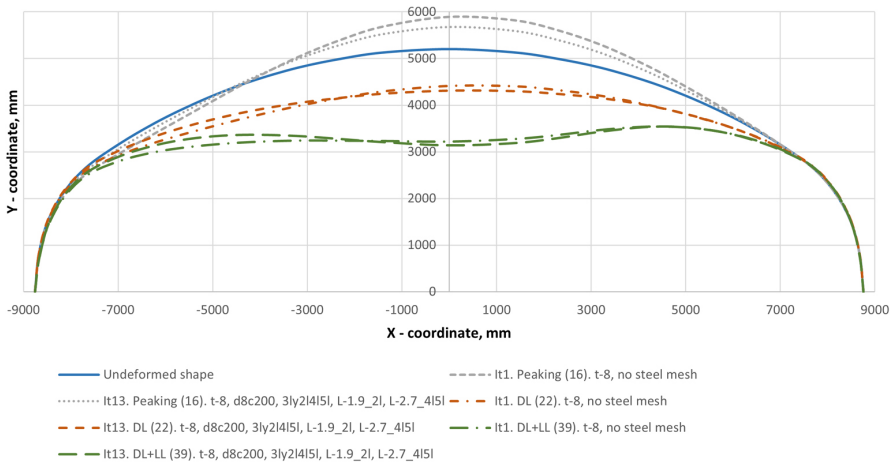
Fig. 6. CSS displacements u_y (mm, scale 1:50) for structure without and with rational steel mesh layout in peaking (16), DL (22) and in the most unfavorable location of LL (39) phase

Displacements are reduced by 45.7% from 13.86 mm to 9.51 mm what generally allows to control structure deformations during soil backfilling on the sides. Meanwhile vertical crown displacements in DL and DL+LL phase is slightly higher for structure with the steel mesh because deformations were already restricted in the peaking phase. However, displacements are higher only by 13.6% in the DL and by 4% in the DL+LL phase accordingly. In addition, the steel mesh unifies structure cross section deformations because of unsymmetrical loading. It is important to mention that displacements are corrected by the mean settlement of the supports. Steel mesh influence on support settlements is minor and up to 1.5% higher.

Figure 7 shows axial force distribution in the cross section of the structure with and without steel meshes.
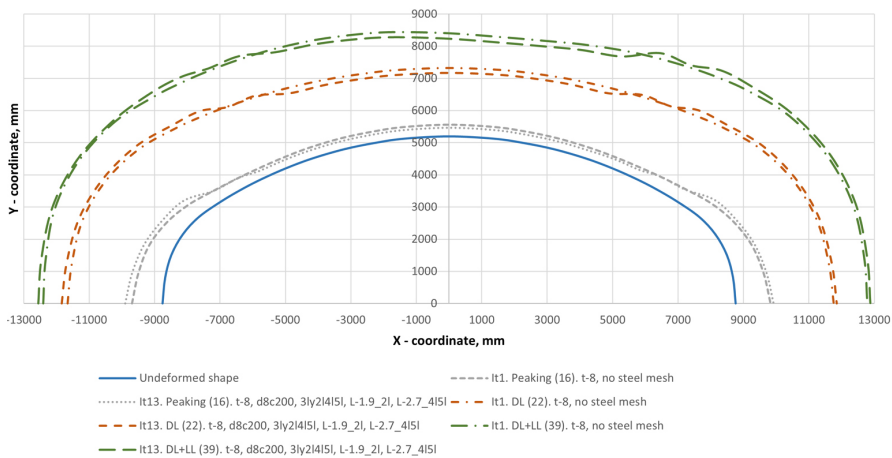
Fig. 7. CSS axial forces (kN/m, scale 1:5) for structure without and with rational steel mesh layout in peaking (16), DL (22) and in the most unfavorable location of LL (39) phase

According to FEM results rational steel meshes layout works in the favor of the crown of the structure because axial force value in the crown is lower by 34.2% in the peaking phase and by 5.7% in the DL+LL phase. However, calculated axial force in the support point is opposite and on the left side of the structure it is higher by 21.7% in the peaking phase and by 4.3% in the DL+LL phase of the structure with steel meshes. Figure 7 also shows a few peaks of redistribution of axial force at the points where steel mesh is connected to the barrel of the structure. Such points could be critical for CSS global stability and must be considered during the design.

Bending moment in the cross section of the structure is visualized in Fig. 8.

Steel mesh influence on CSS is obvious. Bending moments are reduced by steel meshes in the crown and haunches of the structure during the peaking phase. While in the full dead load bending moments are unified by steel meshes and accordingly increased in the crown and reduced in the middle point of the haunches. Almost the same behavior of distribution of bending moments is in the DL+LL phase. The impact of steel meshes is significant and could be utilized to control internal reactions of the structure when necessary. Nevertheless, constraint of CSS by steel meshes should be done responsibly in order not to limit its bearing capacity.
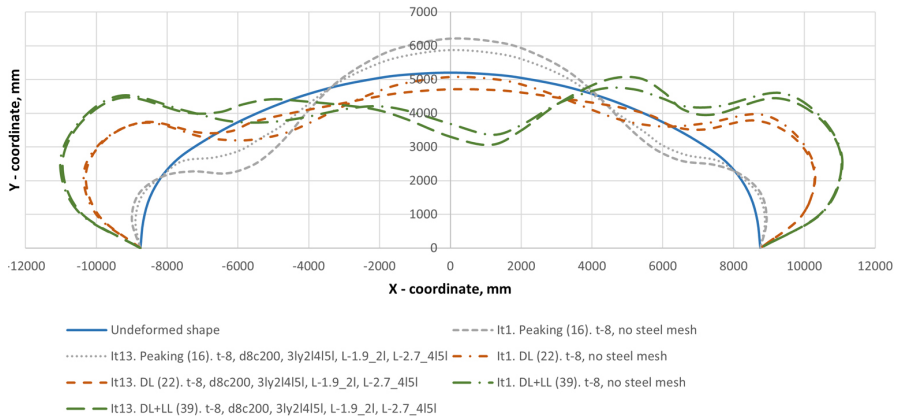
Fig. 8. CSS bending moments (kNm/m, scale 1:30) for structure without and with rational steel mesh
layout in peaking (16), DL (22) and in the most unfavorable location of LL (39) phase

4.3. Steel plate utilization

Steel plate utilization was calculated evaluating only the nature of steel plate buckling
failure according to the Eurocode [39] and AASHTO [3] regulations in the ultimate limit state
(ULS). Utilization results for all calculated iterations are presented below. According to the
peaking phase results by the Eurocode [39] presented in Fig. 9 steel mesh layer closer to the
foundation has a higher influence than layers closer to the crown of the structure.
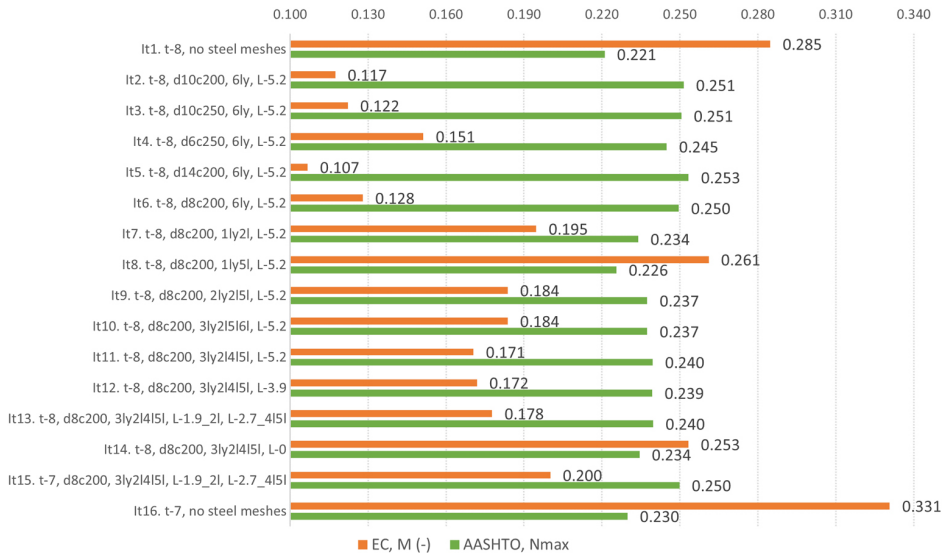
Fig. 9. Utilization of cross section buckling capacity acc. to Eurocode and AASHTO regulations in
peaking (16) phase

In iteration number 7, when only one steel mesh layer is activated in the second level utilization is lower than in iteration No 8 with one steel mesh layer at the fifth level. Such results could be explained considering that structure's crown in the peaking phase moves upward because of the side backfilling pressure and active steel mesh layer at the second level constrain CSS deformations. While one steel mesh layer at 5th level does not have same effect and utilization is higher but still a little bit lower compared with a structure without any steel mesh layers as in iteration No 1. Taking into consideration such steel mesh influence on CSS the positive effect of using steel meshes could be reached when peaking phase is the most critical phase for bearing capacity of the structure. Steel meshes could be used to control excessive CSS deformations, internal forces, and utilization in the peaking phase. Unfortunately, as shown in Fig. 7, steel meshes increase the value of axial forces closer to foundations, so calculation results according to AASHTO [3] shown in Fig. 9 do not present any positive effect for the behavior of CSS.

Calculation results demonstrated in Fig. 10 are prepared in the full DL phase.
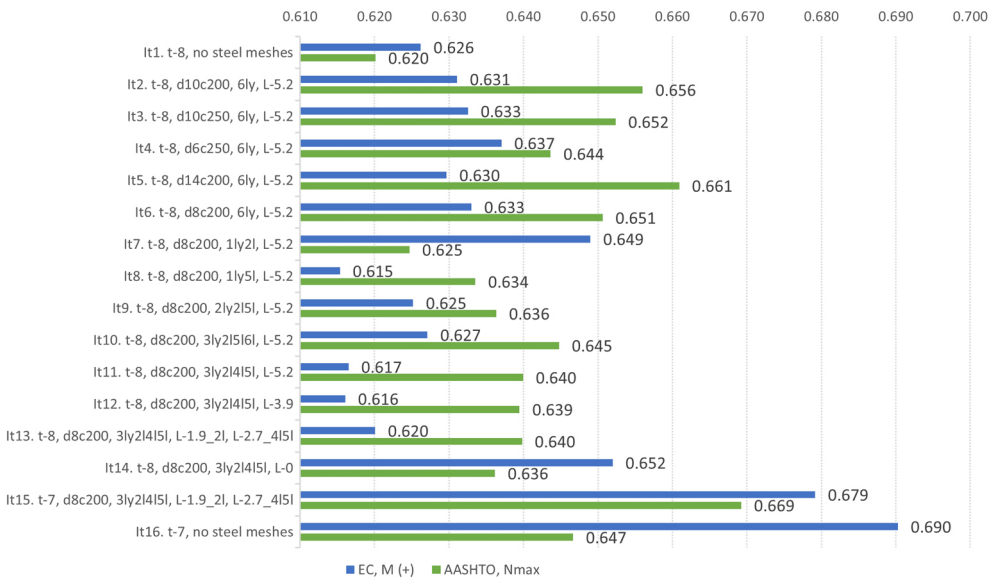
Fig. 10. Utilization of cross section buckling capacity acc. to Eurocode and AASHTO regulations in full DL (22) phase

Contrary to the results in the peaking phase the most significant steel mesh layers are closer to the crown of the structure as shown in iteration No 8 while steel mesh layers which are closer to the foundation lose their advantage. Like during the peaking phase, the crown of the structure moves upward, so under soil backfilling pressure over the crown structure starts to deform inwards and consequently steel mesh layers at the sides of the structure are relaxed and experience potential compression. If peaking phase is not an issue for CSS stability, then steel mesh layers closer to the foundation are not so necessary. In any case, the buckling of steel meshes could be neglected because as results show the steel meshes which experience

compression never return to tension stage in the following phases. Nevertheless, according to EC [39] calculations rational steel mesh combination as in iteration No 13 has very low positive influence on CSS utilization compared with a result of the structure without any steel mesh layers. Moreover, according to AASHTO [3] results plate with active steel meshes utilization is again higher.

Figure 11 presents CSS global stability results from the most unfavorable position of DL+LL loading.
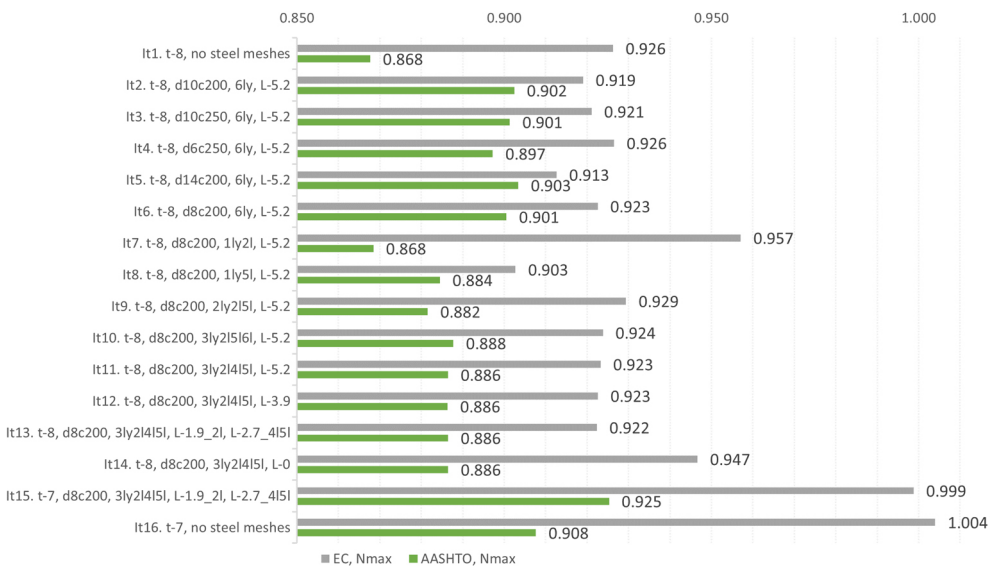
Fig. 11. Utilization of cross section buckling capacity acc. to Eurocode and AASHTO regulations in most unfavorable location of LL (39) phase

The main objective of these results was to understand does steel meshes will increase bearing capacity of the structure sufficiently to reduce its plate thickness. If to analyze iteration No 13 results CSS behavior is similar as in the DL phase. Utilization under EC [39] regulations is slightly lower, however, steel meshes have negative influence on cross section buckling capacity calculated according to AASHTO [3] requirements. If bearing capacity because of the influence of steel meshes does not exceed the limit, then steel meshes still could be used to control CSS behavior when necessary. In specific case, for example as shown in iteration No 15 and No 16, steel meshes could be a decisive factor for CSS bearing capacity. Structure profile analyzed in this study with plate thickness of 7 mm would not satisfy cross section capacity without an impact of steel meshes according to EC [39] approach. While at the same time buckling capacity according to AASHTO [3] would be still in the limit. In addition, Fig. 9, Fig. 10 and Fig. 11 show steel mesh type, quantity, and anchorage length influence on CSS behavior and so redistribution of internal forces because of steel mesh could be generalized in contrast to the results shown in Fig. 6, Fig. 7 and Fig. 8.

5. Conclusions

In the current study, a two-dimensional numerical model of a large span deepest CSS interaction with a different layout of steel meshes were analyzed to present their influence on CSS behavior. All in all, 16 numerical models (iterations) were studied based on nonlinear finite element model of 17.5 m span structure with deepest corrugation of 500×237 mm. Two radius profile buckling capacity was calculated according to Eurocode [39] and AASHTO [3] regulations and compared in the peaking phase, DL phase and in the most unfavorable location of LL phase. Conclusions which could be made from the presented results are listed below:

- CSS crown vertical displacements are mostly restricted by rational layout of steel meshes in the peaking phase. Displacements were reduced by 45.7% allowing to control structure deformations during soil backfilling on the sides of the structure. Moreover, steel meshes unify structure cross section deformations because of unsymmetrical loading.
- Axial force in the crown of the structure could be reduced using rational steel mesh layout from 34.2% in the peaking phase to 5.7% in the most unfavorable position of LL phase. Nevertheless, almost by the same amount axial force is increased at the supports of CSS when steel meshes are activated.
- According to the presented results steel meshes could be a decisive factor for CSS bearing capacity. Following EC [39] approach the profile with 7 mm plate analyzed in this study would lose its stability without constraint of steel meshes. While buckling capacity according to AASHTO [3] would be still in the limit. Cost analysis of equivalent technical solutions (the use of steel mesh or just thicker plate) could be the main objective for future research.
- Steel meshes could be utilized to control internal reactions of the CSS. On the other hand, constraint should be well estimated to avoid negative influence on bearing capacity of the shell of the structure.
- According to FEM results even a very small steel mesh anchorage length (located only in the active zone) had an influence on CSS behavior. Such FEM results are questionable considering embankment over the structure settlements because of structure itself deformations. Such behavior could be justified or rejected by the field test results.
- If the peaking phase is not an issue for CSS plate utilization, steel mesh layers closer to the foundation could be neglected. In addition, according to EC [39] calculations rational steel mesh layout has very low positive influence on CSS global stability under soil pressure in the DL phase. Moreover, CSS with steel meshes plate utilization is even higher according to AASHTO [3] calculation results.
- The quantity of steel mesh layers and anchorage length have minor influence on their utilization to maximum tension force. The diameter and spacing of longitudinal steel bars controls steel meshes resistance to tension. However, according to the results steel mesh layers which experienced the highest tension force were at the level of highest CSS displacements accordingly in the peaking and in the most unfavorable location of LL phase.

References

[1] A.W. Skempton, *Biographical Dictionary of Civil Engineers, Vol. 1: 1500–1830*. London: Thomas Telford, 2002.

[2] CAN/CSA-S6-14 Canadian Highway Bridge Design Code. Canadian Standards Association, 2019.

[3] AASHTO LRFD Bridge Design Specification. American Association of State Highway and Transportation Officials, 2019.

[4] L. Pettersson and A. Wadi, "Structural capacity of existing buried flexible culverts Swedish design methodology", *Archiwum Instytutu Inżynierii Lądowej*, vol. 23, pp. 229–236, 2017, doi: 10.21008/j.1897-4007.2017.23.21.

[5] L. Pettersson, E. B. Flener, and H. Sundquist, "Design of soil-steel composite bridges", *Structural Engineering International*, vol. 25, no. 2, pp. 159–172, 2015, doi: 10.2749/101686614X14043795570499.

[6] L. Pettersson and H. Sundquist, *Design of soil steel composite bridges*. TRITA-BKN, Report 112, 5th ed. KTH Royal Institute of Technology, 2014.

[7] K. Embaby, M.H. El Naggar, and M. El Sharnouby, "Performance of large-span arched soil–steel structures under soil loading", *Thin-Walled Structures*, vol. 172, 2022, doi: 10.1016/j.tws.2022.108884.

[8] A. Wysokowski, "Full scale tests of various buried flexible structures under failure load", *Scientific Reports*, vol. 12, no. 1, 2022, doi: 10.1038/s41598-022-04969-7.

[9] C. Machelski, M. Sobótka, and S. Grosel, "Displacements of shell in soil-steel bridge subjected to moving load: Determination using strain gauge measurements and numerical simulation", *Studia Geotechnica et Mechanica*, vol. 44, no. 1, pp. 26–37, 2022, doi: 10.2478/sgem-2021-0028.

[10] C. Machelski, P. Tomala, and M. Mońka, "Research on the interface elements in soil-steel structures based on the in situ test", in *Modern Trends in Research on Steel, Aluminium and Composite Structures*. Taylor & Francis, 2021, pp. 106–112, doi: 10.1201/9781003132134-10.

[11] W. Fu, X. Fu, Y. He, and B. Li, "Experimental study on mechanical properties of a medium size box-type corrugated steel bridge", in *Advances in Transdisciplinary Engineering, vol. 19: Hydraulic and Civil Engineering Technology VI*. IOS Press BV, 2021, pp. 142–156, doi: 10.3233/ATDE210161.

[12] C. Machelski and L. Korusiewicz, "Contact interaction between corrugated steel shell and the soil backfill determined based on the measurements of shell deformations", *Archives of Civil Engineering*, vol. 67, no. 1, pp. 57–79, 2021, doi: 10.24425/ace.2021.136461.

[13] C. Machelski, "Characteristic changes the bending moments in shell of soil-steel structures", *Transportation Overview*, no. 1, pp. 32–40, 2021.

[14] B. Liu, H. Sun, W. Xu, Y. Shi, B. Zhang, and M. Yao, "Research on the law of stress development along backfilling process between crest and valley of buried corrugated steel pipe culverts", *International Journal of Steel Structures*, vol. 21, pp. 142–153, 2021, doi: 10.1007/s13296-020-00422-5.

[15] W. Liu, X. Wang, H. Jiang, W. Ding, and Q. Zhang, "Monitoring and numerical simulation analysis of corrugated steel support in weak surrounding rock mountain tunnels", *IOP Conference Series: Materials Science and Engineering*, vol. 741, art. no. 012042, 2020, doi: 10.1088/1757-899X/741/1/012042.

[16] M. Miśkiewicz, B. Sobczyk, and P. Tysiac, "Non-destructive testing of the longest span soil-steel bridge in Europe-field measurements and FEM calculations", *Materials*, vol. 13, no. 16, 2020, doi: 10.3390/MA13163652.

[17] A. Andersson and R. Karoumi, "A soil-steel bridge under high-speed railways", *Archiwum Instytutu Inżynierii Lądowej*, no. 23, pp. 45–52, 2017, doi: 10.21008/j.1897-4007.2017.23.04.

[18] L. Pettersson, "Full scale tests and structural evaluation of soil steel flexible culverts with low height of cover", Ph.D. thesis, Royal Institute of Technology (KTH), Stockholm, Sweden, 2007.

[19] A. Wadi, L. Pettersson, and R. Karoumi, "FEM simulation of a full-scale loading-to-failure test of a corrugated steel culvert", *Steel and Composite Structures*, vol. 27, no. 2, pp. 217–227, 2018, doi: 10.12989/scs.2018.27.2.217.

[20] A. Andersson, H. Sundquist, and R. Karoumi, "Full scale tests and structural evaluation of soil-steel flexible culverts for high-speed railways", presented at Second European conference on Buried Flexible Steel Structures, Rydzyna 2012.

[21] A. Wadi, L. Pettersson, and R. Karoumi, "On predicting the ultimate capacity of a large-span soil–steel composite bridge", *International Journal of Geosynthetics and Ground Engineering*, vol. 6, no. 4, 2020, doi: 10.1007/s40891-020-00232-z.

[22] B. Kunecki, "Full-scale test of corrugated steel culvert and FEM analysis with various static systems", *Studia Geotechnica et Mechanica*, vol. 28, no. 2, 2006.

[23] E. Nakhostin, S. Kenny, and S. Sivathayalan, "Numerical performance assessment of buried corrugated metal culvert subject to service load conditions", *Canadian Journal of Civil Engineering*, vol. 48, no. 2, pp. 99–114, 2021, doi: 10.1139/cjce-2019-0316.

[24] D. Beben, "The role of backfill quality on corrugated steel plate culvert behaviour", *Baltic Journal of Road and Bridge Engineering*, vol. 12, no. 1, pp. 1–11, 2017, doi: 10.3846/bjrbe.2017.01.

[25] S. Kenny and S. Sivathayalan, "Examination of buried corrugated metal culvert failure mechanisms using finite elements methods", presented at GeoOttawa 2017: Proceedings of 70th Canadian Geotechnical Conference, Ottawa, Canada, 2017.

[26] A. Wadi, L. Pettersson, and R. Karoumi, "Flexible culverts in sloping terrain: Numerical simulation of soil loading effects", *Engineering Structures*, vol. 101, pp. 111–124, 2015, doi: 10.1016/j.engstruct.2015.07.004.

[27] A. Wadi, L. Pettersson, and R. Karoumi, "Flexible culverts in sloping terrain: Numerical simulation of avalanche load effects", *Cold Regions Science and Technology*, vol. 124, pp. 95–109, 2016, doi: 10.1016/j.coldregions.2016.01.003.

[28] D. Beben and A. Stryczek, "Numerical analysis of corrugated steel plate bridge with reinforced concrete relieving slab", *Journal of Civil Engineering and Management*, vol. 22, no. 5, pp. 585–596, 2016, doi: 10.3846/13923730.2014.914092.

[29] C. Machelski and M. Mumot, "Corrugated shell displacements during the passage of a vehicle along a soil-steel structure", *Studia Geotechnica et Mechanica*, vol. 38, no. 4, pp. 25–32, 2016, doi: 10.1515/sgem-2016-0028.

[30] K. Embaby, M. Hesham El Naggar, and M. El Sharnouby, "Investigation of bevel-ended large-span soil-steel structures", *Engineering Structures*, vol. 267, 2022, doi: 10.1016/j.engstruct.2022.114658.

[31] A. Wysokowski, "Influence of single-layer geotextile reinforcement on load capacity of buried steel box structure based on laboratory full-scale tests", *Thin-Walled Structures*, vol. 159, 2021, doi: 10.1016/j.tws.2020.107312.

[32] D. Beben and Z. Manko, "Static tests on a soil - Steel bridge structure with a relieving slab", *Structure and Infrastructure Engineering*, vol. 6, no. 3, pp. 329–346, 2010, doi: 10.1080/15732470701511618.

[33] P. Tomala and R. Vegerby-Hansen, "Structure in big skew - Gladsaxe case Denmark", *Archiwum Instytutu Inżynierii Lądowej*, no. 23, pp. 279–286, 2017, doi: 10.21008/j.1897-4007.2017.23.25.

[34] T. Maleska and D. Beben, "Numerical analysis of a soil-steel bridge during backfilling using various shell models", *Engineering Structures*, vol. 196, 2019, doi: 10.1016/j.engstruct.2019.109358.

[35] Bentley, "Plaxis 2D Geotechnical Engineering Software". [Online]. Available: https://www.bentley.com/software/plaxis-2d/. [Accessed: 15. November. 2023].

[36] J. G. Potyondy, "Skin friction between various soils and construction materials", *Géotechnique*, vol. 11, no. 4, pp. 339–353, 1961, doi: 10.1680/geot.1961.11.4.339.

[37] M. A. Legese, M. Sobotka, C. Machelski, and A. Rozanski, "Behaviour of soil-steel composite structures during construction and service: a review", *Archives of Civil Engineering*, vol. 69, no. 4, pp. 263–292, 2023, doi: 10.24425/ace.2023.147659.

[38] M. G. Katona, "Improved methods for simulating live loads for two-dimensional structural analysis of buried culverts", *Transportation Research Record*, vol. 2673, no. 12, pp. 449–462, 2019, doi: 10.1177/0361198119846465.

[39] EN 1993-2:2006 Eurocode 3 Design of steel structures - Part 2: Steel bridges. European Standard, 2006.

[40] BS 8006-1 :2010+A1:2016 Code of practice for strengthened/reinforced soils and other fills. British Standard, 2016.